Volume 1 | Number 1 | Jan 2013 | Pages 1–100

ROYAL SOCIETY OF CHEMISTRY

ROYAL SOCIETY OF CHEMISTRY

www.rsc.org/catalysis

Journal Name

A stable, efficient 3D Cobalt-graphene composite catalyst for the hydrolysis of ammonia borane

Mengxiong Li,[a,b] Jiantong Hu [a,b] and Hongbin Lu [a,b] *

Low-cost, stable and highly efficient catalysts are essential for practical energy applications. In this study, branched polyethylenimine (PEI)-decorated graphene oxide (GO) 3D structures were prepared through the hydrothermal reaction. Cobalt (Co) nanoparticles (NPs) were deposited on PEI-GO 3D structures, forming a desired, low-cost composite catalyst PEI-GO$_{3D}$/Co. The catalyst shows a quite high catalytic activity for the room temperature hydrolysis of ammonia borane, with a turnover frequency of 18.5 mol$_{H_2}$ min^{-1} mol$^{-1}_{Co}$ and a hydrogen generation rate of 7.68 L$_{H_2}$ min^{-1} g$^{-1}_{Co}$. The activation energy of the catalyst is relatively low (27.41 kJ mol^{-1}), along with an ultrahigh cycle stability, that is, ~ 83% of the initial catalytic activity was retained after 5 catalytic cycles, superior to the majority of non-noble metal catalysts.

1. Introduction

Significantly increased energy demands drive one to explore new energies that can reduce the consumption of fossil energy. Hydrogen is an ideal energy for future applications due to lots of advantages, such as clean and high value of combustion heat.[1,2] Hydrogen production through water splitting has attracted lots of attentions,[3-5] however, it is confined to some extent by the lack of high capacity hydrogen storage materials and satisfactory production efficiency. Therefore, how to achieve highly efficient production and storage of hydrogen has been the focus of many efforts. Ammonia borane (NH$_3$BH$_3$, AB) is a kind of chemical hydrogen storage material with high hydrogen capacity (19.6 wt%), chemical stability, non-toxicity and high water solubility.[6] The hydrolysis of AB to produce hydrogen happens around room temperature under the assistance of catalysts, with a relatively fast dehydrogenation rate usually. This has thus attracted considerable attention to develop a variety of highly efficient catalysts for practical applications of hydrogen energy.[7,8]

Noble metals (e.g., Pt, Ru, Rh)[9-11] and non-noble metals (e.g., Fe, Co, Ni)[12-14] are mostly used as catalysts for AB hydrolysis. Non-noble metals are cheap and abundant in nature, and thus more suitable for various practical applications, despite their relatively low activities as opposed to those noble metals. Among non-noble metal catalysts, Co-based catalysts show much higher catalytic activities, even comparable to that of some noble metal catalysts. Nevertheless, it remains challenging how to achieve good stability for these highly active no-noble metal catalysts. Therefore, much effort has been

made to improve simultaneously the activity and stability of metal catalysts. For metal catalysts, increased particle sizes are undesired and result in reduced catalytic activities, causing the aggregation during the catalytic reaction. The result has been verified by TEM characterization.[15-17] In addition, XPS characterization also confirms that non-noble metal NPs could be oxidized during the reaction, because of their inevitably contact with oxidants like oxygen in the process of use or stability tests.[18-20] To address these issues, one possible approach is to form bimetallic systems with other metals. The synergistic effect between two metals can significantly increase the catalytic activity, and well-designed structures (e.g., core-shell, alloy, etc.) can also improve the stability of the catalyst.[11,14,16,21] However, such catalysts usually require special structures and precise facet control to achieve high activity and stability, which are usually difficult for practical applications.[22] On the other hand, these metal NPs have normally high surface energies that cause aggregation or oxidization in the absence of protective agents, and reduced active sites. In this regard, depositing metal NPs on suitable supports could be effective in preventing from aggregation, restricting the contact with oxidants.

Generally, the supports of NPs should be stable in the catalytic reaction and have high specific surface areas (SSA), e.g., active carbon[23] and SiO$_2$.[24] Graphene is a two-dimensional plate-like carbon film with the thickness of single carbon atom. The high SSA (2630 m^2 g^{-1}) and extraordinary physical/chemical properties enable it to be an ideal candidate as supporting materials for catalysts. Also, graphene may interact directly with metal NPs to enhance the electron transfer efficiency and catalytic activity.[19,25] However, both size and spatial distributions of metal NPs deposited directly on graphene are uneven usually, and the flat structure of graphene sheets cannot effectively prevent the aggregation of metal NPs. The stability of graphene-metal NPs composite catalysts is also limited.[8,26] Decorating GO with various polymers has become a

[a.] State Key Laboratory of Molecular Engineering of Polymers, Collaborative Innovation Center of Polymers and Polymer Composite Materials and Department of Macromolecular Science, Fudan University, Shanghai 200433, China
[b.] Shanghai Xiyin New Materials Corporation, 135 Guowei Road, Shanghai, 200438, China

good choice to disperse metal NPs and avoid aggregation.[27,28] Branched PEI has numerous amine groups, and can be easily adsorbed or grafted on graphene through the chemical reaction and form desired structures.[29] In our previous work,[30] we found that the amine groups of PEI decorated GO could not only disperse Co NPs, but may also provide some synergistic effect, leading to significantly increased catalytic activity. Nevertheless, the stability of the catalyst PEI-GO/Co is still highly limited, after 5 catalytic reactions, it lost ~40% of the initial catalytic activity, limiting its practical application. If the support contains 3D porous structures, metal NPs dispersed inside the support will be well protected, resulting in improved stability.[18] However, this could decreases the catalytic activity of the catalyst due to reduced contact between metal NPs active centers and reactants.[31] Nonetheless, such 3D structure-supported metal catalysts practically open an important direction for optimizing performance of metal catalysts.

In this work, we construct well-designed 3D structures of PEI-GO with a large amount of amine groups and exhibit their excellent dispersion ability for Co NPs. The obtained PEI-GO$_{3D}$/Co shows good catalytic activity with a TOF value of 18.5 mol$_{H_2}$ min^{-1} mol$^{-1}_{Co}$, a hydrogen generation rate of 7.68 L$_{H_2}$ min^{-1} g$^{-1}_{Co}$, along with significantly improved cycle stability. After 5 cycles of catalytic reactions, only ~17% of its initial catalytic activity is lost, far superior to the majority of the results reported of non-noble metal catalysts. In addition, our results further confirm that amine groups can provide a synergistic effect to Co NPs and dramatically increase the catalytic activity, demonstrating a novel, highly efficient method for simultaneous optimization of activity and stability of AB hydrolysis catalysts.

2. Experimental

2.1 Chemicals

Graphite powder 8099200 (120 μm) was obtained from Qingdao BCSM. 50% hydrazine hydrate (N$_2$H$_4$•H$_2$O), 65% nitric acid (HNO$_3$), 98% sulfuric acid (H$_2$SO$_4$), 30% hydrogen peroxide (H$_2$O$_2$) and 96% sodium borohydride (NaBH$_4$) were purchased from Sinopharm Chemical Reagent Company. Sodium nitrate (NaNO$_3$) was got from Shanghai Qiangshun Chemical Company, potassium hypermanganate (KMnO$_4$) was obtained from Shanghai Zhenxing Chemical Company, PEI (M$_w$ = 600, branched) and cobalt (II) acetate tetrahydrate (Co(Ac)$_2$•4H$_2$O) were purchased from Alfa Aesar. AB was obtained from Sigma Aldrich. Deionized water was used in all experiments. All chemicals were used as received.

2.2 Synthesis of PEI-GO$_{3D}$ and PEI-GO$_{2D\ amide}$

GO was prepared by the Hummers' method and freeze-dried before use. Typically, 1g graphite and 0.75 g NaNO$_3$ were added into 23 mL H$_2$SO$_4$, followed by the slow addition of 3g KMnO$_4$. These reactants were kept at 35 °C for 45 min with magnetic stirring. Subsequently, 46 mL deionized water was added and the mixture was kept at 98 °C for 15 min to which 140 mL deionized water and 10 mL H$_2$O$_2$ were then quickly added. The obtained GO was purified and freeze-dried. After freeze-drying,

50 mg GO was dissolved in 10 mL deionized water with sonication of 30 min to form dark-brown solution. After that, 10 mL deionized water containing 500 mg PEI was slowly added into the GO solution. The mixture was then magnetically stirred at 60 °C for 12 h and then transferred into a 25 mL autoclave and heated at 180 °C for 12 h. After the hydrothermal reaction, the obtained PEI-GO$_{3D}$ was purified by centrifugation and freeze-dried for further use.

PEI-GO$_{2D\ amide}$ was prepared according to the following procedure. 50 mg GO was dissolved in 10 mL deionized water with sonication of 30 min. Then 10 mL deionized water containing 500 mg PEI was slowly added into the GO solution. The pH value of the mixed solution was tuned to 7. Then the mixture was magnetically stirred at 60 °C for 12 h. The product was purified by centrifugation and freeze-drying.

2.3 Synthesis of the catalysts PEI-GO$_{3D}$/Co and PEI-GO$_{2D\ amide}$/Co

PEI-GO-based catalysts were synthesized by deposition of Co NPs on the support. Typically, 10 mg as-prepared PEI-GO$_{2D\ amide}$ or PEI-GO$_{3D}$ was dispersed in 20 mL deionized water with sonication of 15 min in a two-necked round-bottom flask. 0.2 mmol Co(Ac)$_2$ was then added. The mixture was magnetically stirred for 30 min under N$_2$ atmosphere. 20 mg NaBH$_4$ was then added into the mixture. After completing the reduction reaction, the obtained PEI-GO$_{2D\ amide}$/Co or PEI-GO$_{3D}$/Co was collected at the bottom by using a magnet, washed with deionized water and dried naturally under N$_2$ atmosphere.

2.4 Catalytic hydrolysis of AB

When the catalyst was dried, 18 mL deionized water was directly added into the flask. After sonication for 15 min, 2 mL deionized water containing 1.5 mmol AB was injected into the solution with a magnetic stirring of 1200 rpm. The catalytic reaction was carried out under the ambient condition. The volume of H$_2$ generated was monitored with a gas burette. To carry out the cycle test, the catalyst was collected at the bottom of the flask with a magnet after completing the hydrolysis, and the supernatant solution was carefully removed. After washing the catalyst, 18 mL deionized water was added and 2 mL deionized water containing 10 mg AB was injected for the cycle test. The same process was repeated five times. To study the kinetics of the catalytic reaction, different concentrations of PEI-GO$_{3D}$/Co (2.5, 5.0, 7.5, 10.0 mmol L^{-1}) were prepared for the dehydrogenation examination of 1.5 mmol AB. To study the effect of temperature, the catalytic reaction was performed at 25, 35, 45, 55 °C, respectively.

2.5 Characterization

Transmission electron microscopy (TEM, Jeol JEM-2100F and Tecnai G^2 TF20 Twin, both operating at 200 kV) was used to observe the morphology of PEI-GO/Co. The field emission scanning electron microscopy (FESEM, S-4800 high resolution field emission scanning electron microscopy) was used to observe the structure of the catalysts. Energy dispersive analysis (EDX) was performed on S-4800 FESEM with a Bruker QUANTAX 400 detector. Thermo gravimetric analysis (TGA) was conducted on a PerkinElmer Pyris 1 TGA from 50 to 800 °C at a heating rate of 20 °C min^{-1} under nitrogen atmosphere. X-ray

photoelectron spectra (XPS) was conducted on a Kratos AXIS UltraDLD system
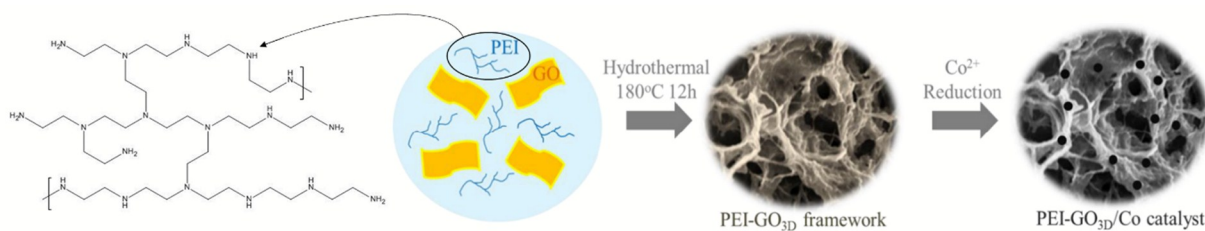
Scheme 1 Synthesis of the PEI-GO_{3D}/Co catalyst.

with monochromatic Al Kα radiation ($h\upsilon$ = 1486.6 eV). Fourier transform infrared spectroscopy (FT-IR) was recorded on a NEXUS 670 spectrometer at room temperature over a frequency range of $750 - 4000$ cm^{-1}. The specific surface area was obtained by using N$_2$-adsorption-desorption method on a Quadrasorb evo system.

3. Results and discussion

The 3D support PEI-GO$_{3D}$ was prepared by a modified method of our previous work,[30] as shown in Scheme 1. GO was first dispersed in deionized water, followed by dropping PEI into the aqueous solution. One example for the structure of branched PEI is presented in Scheme 1. After reaction for 12 h at 60 °C, the mixture was transferred into an autoclave and heated to 180 °C for 12 h. During the hydrothermal reaction, primary and secondary amine groups on branched PEI molecules readily react with carboxyl groups on GO sheets by amidation reaction, to form amide groups.[32] The amide rich PEI-GO$_{2D\ amide}$, as a reference, was synthesized as well following the previous method.[28]

The amount of PEI molecules decorated on GO is measured by TGA, and the corresponding results are shown in Fig. 1a. Around 200 °C, the weight of GO decreases sharply, due to the removal of oxygen functional groups. Beyond 300 °C, the weight loss of GO is not evident. The decomposition of PEI mainly

Fig. 1 (a) TGA curves and (b) FT-IR spectra of GO, PEI, PEI-GO$_{3D}$ composites.

occurs between 300-400 °C. By comparison, PEI-GO$_{3D}$ exhibits a ~45% weight loss between 300-400 °C, suggesting a significant amount of PEI (45%) deposited on GO. However, the content of PEI in PEI-GO$_{2D\ amide}$ is about 30%, as shown in Fig. S1a, which is quite low. The result implies that more amine groups in PEI molecules are converted into amide groups and the carboxyl groups on GO are consumed completely, leading to a low PEI content. Fig. 1b shows the FT-IR spectra of PEI, GO and the PEI-GO$_{3D}$ support. The characteristic peaks at 1730 and 1630 cm^{-1} of GO, corresponding to C=O and C-OH vibrations, are greatly reduced in PEI-GO$_{3D}$. Two obvious peaks at 2958 and 2830 cm^{-1} are ascribed to the asymmetric and symmetric stretching of CH$_2$ on PEI. The peaks at 1574 and 1463 cm^{-1} are NH$_2$ binding peak and C-N stretching vibration peak, respectively. These two peaks reflects the existence of amine groups. At last, the peak at 1658 cm^{-1} of PEI-GO$_{3D}$ indicates the formation of amide bonds, suggesting that part of PEI molecules was covalently linked with GO. But for PEI-GO$_{2D\ amide}$, the peak at 1658 cm^{-1} of is obvious, while two peaks at 1562 (-NH$_2$) and 1463 cm^{-1} (C-N) are nearly invisible. It can be concluded that in PEI-GO$_{2D\ amide}$, the content of amide group is relatively high.

TEM and FESEM were subsequently used to observe the morphology of PEI-GO$_{3D}$, as shown in Fig. 2. Some large folds and corrugations on GO sheets are clearly visible in Fig 2a and 2b, reflecting the influence of PEI molecules on the morphology of GO. The obvious variation on depth of field observed in Fig. 2c and d indicates that PEI-wrapped GO sheets generate porous and 3D structures with a large, accessible SSA. High SSAs, along with the amine groups of PEI, are beneficial for capturing metal ions, leading to uniform deposition and better protection of metal NPs. The N$_2$-adsorption-desorption result shows that the SSA of PEI-GO$_{3D}$ is 240 m^2 g^{-1}, with highly accessible surfaces. In contrast, PEI-GO$_{2D\ amide}$ has a lower SSA, only 196 m^2 g^{-1}, indicating that the sheet stack in PEI-GO$_{2D\ amide}$ probably limits it surface accessibility and dispersing ability for metal NPs. In heterogeneous catalysis, the size and distribution of metal NPs significantly influence the activity of catalysts. The morphology and spatial distribution of NPs in PEI-GO3D/Co is observed by
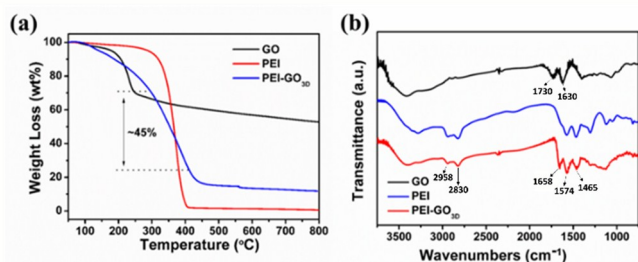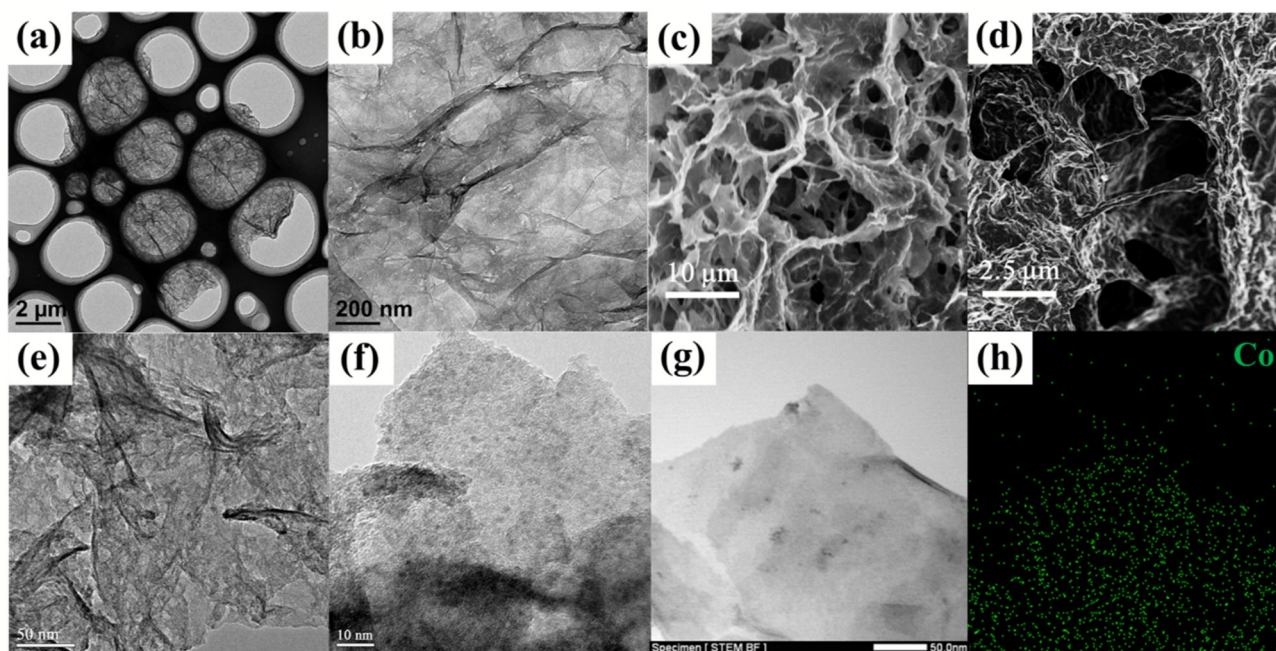
Journal Name

ARTICLE

Fig. 2 (a, b) TEM and (c, d) FESEM images of PEI-GO$_{3D}$ composites. The inset of (c) shows the shape of PEI-GO$_{3D}$ monolithic aerogel obtained after hydrothermal reaction and freeze-drying. (e, f) HRTEM of PEI-GO$_{3D}$/Co, (g) its bright field image under STEM mode, and (h) the corresponding metal element mapping image.
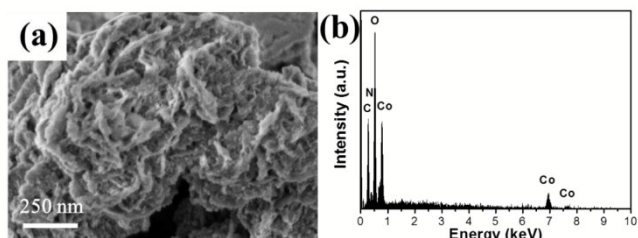

Fig. 3 (a) FESEM image and (b) EDX spectrum of PEI-GO$_{3D}$/Co composites.

HRTEM. In Fig. 2e, the microscopic structures with folds and corrugations are visible. Fig. 2f displays numerous Co NPs compactly distributed on the surface of PEI-GO$_{3D}$, with an average size of 2~3 nm. The bright green spots in the STEM dark field image (Fig. 2h) reflects the spatial distribution of Co NPs on the surface and, the numerous, dense spots further confirm the uniform dispersion of NPs on PEI-GO$_{3D}$. FESEM result of PEI-GO$_{3D}$/Co is shown in Fig. 3 in which the brighter area (composed of white spots) in Fig. 3a represents the Co NPs deposited around the wrinkles generated by PEI, and a porous structure can also be clearly visible. The corresponding EDX spectrum also affords further evidence for the deposition of Co NPs on PEI-GO$_{3D}$, where the composite catalyst is primarily composed of C,

N, O and Co. These results indicate that the obtained catalyst PEI-GO$_{3D}$/Co would have excellent catalytic activity. Fig. S2a shows the TEM image of PEI-GO$_{2D\ amide}$, from which less corrugations are observed. This suggests that less PEI molecules are attached on GO sheets in PEI-GO$_{2D\ amide}$ relative to PEI-GO$_{3D}$, which agrees with the TGA results. From the FESEM image in
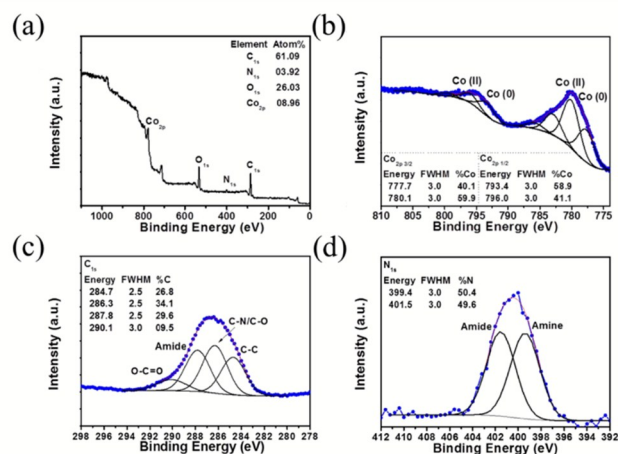

Fig. 4 (a) XPS survey and (b-d) Co$_{2p}$, C$_{1s}$ and N$_{1s}$ core-level spectra of PEI-GO$_{3D}$/Co composites.
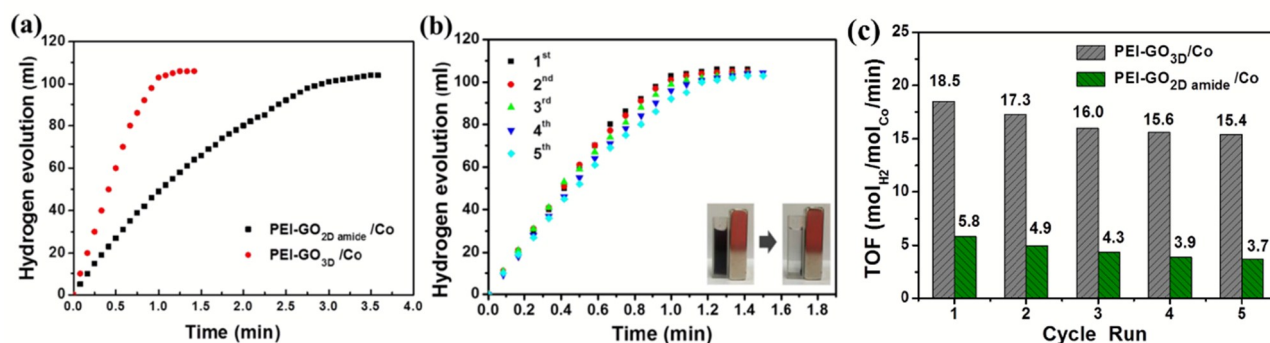
Journal Name

ARTICLE

Fig. 5 Hydrogen generation rate of the AB hydrolysis of PEI-GO$_{3D}$/Co and PEI-GO$_{2D\ amide}$/Co, and (b) hydrogen generation rates in the presence of PEI-GO$_{3D}$/Co with recycling use for 5 times under ambient condition. The inset image of (b) shows the photograph of the catalyst PEI-GO$_{3D}$/Co before and after magnetic separation, and (c) recyclability comparison between PEI-GO$_{3D}$/Co and PEI-GO$_{2D\ amide}$/Co.

Fig. S2b, we find no obvious 3D structure in PEI-GO$_{2D\ amide}$. Fig. S2c, d show that Co NPs on PEI-GO$_{2D\ amide}$ are uniformly distributed, with the average size of ~4 nm and larger than those NPs deposited on PEI-GO$_{3D}$. These results are in accordance with their SSAs, indicating the great advantage of PEI-GO$_{3D}$ as a support.

XPS spectra were used to identify the chemical composition and metal valence state, as shown in Fig. 4. Four prominent band groups appeared at 286, 400, 532 and 780 eV represent the C$_{1s}$, N$_{1s}$, O$_{1s}$ and Co$_{2p}$, respectively. Fig. 4b presents the further details of Co$_{2p}$ characteristic peaks. The peaks at 777.7 and 781.1 eV represent Co (0) species, and peaks at 793.4 and 796.0 eV indicate the existence of Co (II) species. During the XPS test, the catalysts inevitably contact with oxygen in the process of preparing samples. This implies that highly active Co NPs probably formed partially oxidized NPs. Similar results can also be found in the literatures.[18-20] The C$_{1s}$ core-level spectrum in Fig. 4c is fitted using four Gaussian peaks at 284.7, 286.3, 287.8 and 290.1 eV, which may be assigned to C-C, C-N/C-O, C(O)NH and O-C=O species. Up to 30% of functional groups are found to be amide group, suggesting that PEI molecules would be linked covalently on the GO surface. For the N$_{1s}$ core-level spectrum in Fig. 4d, the peaks at 399.4 and 401.5 eV represents amine and amide groups, respectively. Among them, the contribution from amide group takes up about 50%. The content of amide groups has a significant increase compared with that of our previous work (20%),[30] suggesting that during the hydrothermal reaction, the amine groups of PEI molecules can further react with carboxyl groups on GO. The strong interaction between GO and PEI helps form the ideal 3D porous structure of PEI-GO$_{3D}$. For PEI-GO$_{2D\ amide}$, the corresponding XPS results are presented in Fig. S3. For the C$_{1s}$ spectrum, peaks at 284.8 and 288.1 eV reflect C-C and C(O)NH species. For the N$_{1s}$ spectrum, only the

peak at 401.2 eV is observed, indicating that nearly all the functional groups containing N atom are amide groups. The high amide content may explain the major catalytic activity difference between PEI-GO$_{2D\ amide}$/Co and PEI-GO$_{3D}$/Co. Furthermore, No Co(0) specie is obtained for PEI-GO$_{2D\ amide}$ (Fig. S3c). This may be explained by the fact that PEI-GO$_{2D\ amide}$/Co is easier to be oxidized during the sample preparation for XPS characterization than PEI-GO$_{3D}$/Co, suggesting that PEI-GO$_{3D}$/Co would have better stability than that of PEI-GO$_{2D\ amide}$/Co.

Fig. 5a shows the activities of the composite catalysts for AB hydrolysis, where the volumes of H$_2$ generated using different catalysts were recorded. To better demonstrate the catalytic activity of PEI-GO$_{3D}$/Co, a control experiment with PEI-GO$_{2D\ amide}$/Co was conducted as well. Usually, a 3D-structured support may restrict the diffusion of reactants into the internal space due to the separation effect of pore walls, impair the contact probability between the Co NPs and AB molecules, and thus lead to reduced catalytic activities. Surprisingly, however, PEI-GO$_{3D}$/Co exhibits a much better catalytic activity than that of PEI-GO$_{2D\ amide}$/Co (Fig. 5a), in which AB was completely hydrolyzed in 1 min in the presence of PEI-GO$_{3D}$/Co, which is far faster than that (3.5 min) of PEI-GO$_{2D\ amide}$/Co. Given that PEI-GO$_{3D}$ has 50% amine groups but PEI-GO$_{2D\ amide}$ nearly 0%, we suppose that the difference in catalytic activity could arise from their different contents of amine groups. In other words, the amine groups of PEI molecules could play some synergistic role, along with Co NPs, in catalyzing AB hydrolysis, except that the better dispersion ability of 3D porous structure of PEI-GO$_{3D}$ could significantly increase catalytic activity. The TOF value of PEI-GO$_{3D}$/Co is 18.5 mol$_{H2}$ min^{-1} mol$^{-1}_{Co}$, the corresponding hydrogen generation rate reaches 7.68 L$_{H2}$ min^{-1} g$^{-1}_{Co}$, which is quite high for Co-based catalysts according to the comparison results shown in Table 1.

Table 1 The comparison of TOF value, E_a and stability of different catalysts.

Catalysts	TOF $mol_{H2}\,min^{-1}\,mol^{-1}_{metal}$	E_a $kJ\,mol^{-1}$	Stability (5 cycles)	Ref.
PEI-GO$_{3D}$/Co	18.5	27.41	83%	this study
PEI-GO$_{2D\ amide}$/Co	5.8	27.55	63%	this study
Pt@SiO$_2$	158.6	53.9	~93%	[33]
NiCo-Pt	10.8	45.72	~85%	[34]
CuCo@MIL-101	19.6	-	~82%	[35]
Ru@Ni/graphene	31	36.59	~76%	[36]
Co$_{35}$Pd$_{65}$/C	22.7	27.5	~75%	[15]
Co/SiO$_2$	13.2	42	74%	[37]
Ru-Rh/PVP	386	47.4	70%	[38]
Ru/laurate	75	47.0	53%	[39]
Ag@CoNi	15.9	32.6	50%	[40]
Cu$_{0.33}$Fe$_{0.67}$	6.7	43.2	~48%	[41]
Ru/C	70.5	28	24%	[42]

The PEI-GO$_{3D}$/Co also exhibits excellent cycle stability. As shown in Fig. 5b, after 5 catalytic cycles, PEI-GO$_{3D}$/Co retains ~83% of the initial catalytic activity, which is obviously superior to that of PEI-GO$_{2D\ amide}$ (only 63% after 5 cycles, Fig. 5c). Generally, the spontaneous combustion of Co NPs takes place immediately when they are exposed to air. This means that preventing them from contacting with oxidants could be a critical factor to extend the cycle life of Co-based catalysts. The 3D structure of the support can effectively prevent the aggregation and oxidation of Co NPs on it, and thus significantly extend the cycle life of the catalyst. For PEI-GO$_{2D\ amide}$, such a block effect is not obvious compared with PEI-GO$_{3D}$, and Co NPs

Fig. 6 (a) Hydrolysis of AB at different concentration of PEI-GO$_{3D}$/Co catalyst at room temperature and (b) the corresponding Arrhenius plot of ln rate vs. ln [Co].

Fig. 7 (a) Hydrolysis of AB at different temperatures catalysed by PEI-GO$_{3D}$/Coand (b) the corresponding Arrhenius plot of ln rate vs. (1/T).

are easily exposed to impurities or oxidants, leading to fast loss of the catalytic activity. Fig. S4 also give the TEM images of the two catalysts after the stability test. According to the experimental observation, the particle size of PEI-GO$_{3D}$/Co doesn't reveal remarkable change, an average size of ~3 nm is retained. However, for PEI-GO$_{2D\ amide}$/Co, the average size of Co NPs increase from ~4 nm to ~5 nm. This implies that the 3D structure of PEI-GO$_{3D}$ can effectively prevent the metal NPs from aggregation. Apparently, PEI-GO$_{3D}$ exhibits a better advantage in improving the dispersion of metal NPs and catalytic activity. Table 1 compares the activity and stability of a variety of Co-based catalysts. It can be found that the PEI-GO$_{3D}$/Co has higher catalytic activity than Co-based monometallic catalysts, comparable to those Co-based multimetallic catalysts or even noble metal catalysts. Moreover, the stability of PEI-GO$_{3D}$/Co is quite good, superior to many multimetallic or noble metal catalysts, indicating the excellent advantage of PEI-GO$_{3D}$ supports.

To study the kinetics of AB hydrolysis, the catalytic activities of PEI-GO$_{3D}$/Co containing different amounts of catalysts (2.5, 5, 7 and 10 mM) were examined, while keeping other factors constant. The results are shown in Fig. 6a. The hydrogen generation rates (r) for different catalysts were extracted from the liner part of each curve in Fig. 6a and ln(r) versus ln[Co] is plotted in Fig. 6b. A slope of 1.15 suggests that PEI-GO$_{3D}$/Co catalyzed AB hydrolysis nearly can be taken approximately as a first-order reaction. This is consistent with the previous reports, indicating that the hydrogen generation rate of the AB hydrolysis is controlled primarily by the surface reaction. The apparent rate constant would be proportional to the total surface area of active sites for surface controlled reaction.[43] As a result, the high catalytic activity of PEI-GO$_{3D}$/Co would arise from the increased active surface sites of Co NPs.

To study the effect of temperature on the PEI-GO$_{3D}$/Co–catalyzed AB hydrolysis, a series of experiments were conducted at different temperatures (25, 35, 45 and 55 °C). As
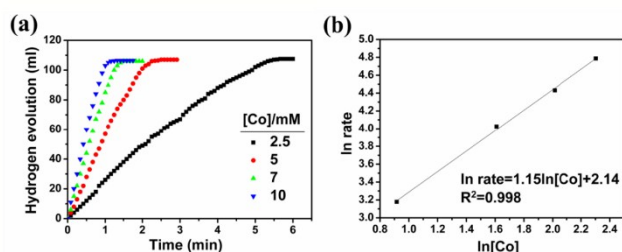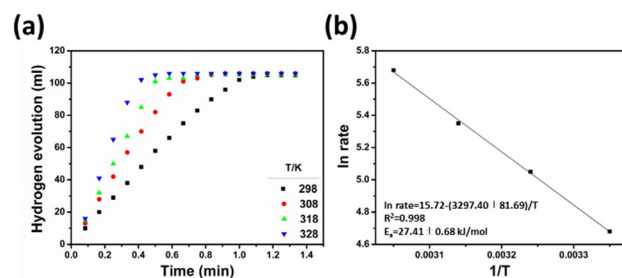
shown in Fig. 7, the hydrogen generation rate (r) increases with the rise of temperature, which was calculated from the linear part of the curve at each temperature. Subsequently, ln(r) verses 1/T is re-plotted in Fig. 7b. Based on the Arrhenius equation, an apparent activation energy of 27.41 ± 0.68 kJ mol^{-1} for the PEI-GO$_{3D}$/Co-catalyzed AB hydrolysis was obtained, which is lower than those of other Co-based catalysts, as shown in Table 1, indicating the excellent catalysis activity of the PEI-GO$_{3D}$/Co composite catalyst and a special catalytic reaction route of amine-rich PEI-GO$_{3D}$/Co catalyst.[30]

4. Conclusions

We have demonstrated the excellent activity and cycle stability of the 3D structured PEI-GO$_{3D}$/Co composite catalyst for the catalytic hydrolysis of AB. Due to the porous 3D structure, high SSA and stable chemical properties, PEI-GO$_{3D}$ allows to load size-controlled metal NPs, and prevents them from aggregation and oxidation. More importantly, a large amount of amine groups in PEI-GO$_{3D}$ provide a synergistic effect to Co NPs, resulting in significant improvement in catalytic activity and cycle stability. The PEI-GO$_{3D}$/Co composite catalyst exhibits a TOF value of 18.5 mol$_{H2}$ min^{-1} mol^{-1}$_{Co}$, a hydrogen generation rate of 7.68 L$_{H2}$ min^{-1} g^{-1}$_{Co}$, and a low activation energy of 27.41 kJ mol^{-1}. Moreover, it can keep 83% of the initial catalytic activity after 5 cycles. These excellent properties are superior to the majority of multimetallic Co-based catalysts, even comparable to those of some noble metal catalysts. Such a low-cost, highly active and stable PEI-GO$_{3D}$/Co catalyst exhibits great potential for practical energy applications.

Acknowledgements

References

1   Schlapbach and A. Züttel, *Nature*, 2001, **414**, 353.
2   M. S. Dresselhaus and I. L. Thomas, *Nature*, 2001, **414**, 332.
3   J. F. Xie, J. J. Zhang, S. Li, F. Grote, X. D. Zhang, H. Zhang, R. X. Wang, Y. Lei, B. Pan and Y. Xie, *J. Am. Chem. Soc.*, 2013, **135**, 17881.
4   T. T. Jia, A. Kolpin, C. S. Ma, R. C.-T. Chan, W.-M. Kwok and S. C. E. Tang, *Chem. Commun.*, 2014, **50**, 1185.
5   J. D. Benck, Z. B. Chen, L. Y. Kuritzky, A. J. Forman and T. F. Jaramillo, *ACS Catal.*, 2012, **2**, 1916.
6   U. B. Demirci and P. Miele, *Energy Environ. Sci.*, 2009, 2, 627.
7   F. H. Stephens, V. Pons and R. T. Baker, *Dalton Trans.*, 2007, **25**, 2613.
8   M. Chandra and Q. Xu, *J. Power Sources*, 2006, **156**, 190.
9   S. G. Peng, J. C. Liu, J. Zhang and F. Y. Wang, *Int. J. Hydrogen Energy*, 2015, **40**, 10856.
10   Q. L. Yao, Z. H. Lu, Y. S. Jia, X. S. Chen and X. Liu, *Int. J. Hydrogen Energy*, 2015, **40**, 2207.
11   J. J. Zhang, T. Wang, X. L. Xu, P. Xiao and J. L. Li, *Appl. Catal. B-Environ.*, 2013, **130-131**, 197.
12   Q. L. Yao, Z. H. Lu, Y. Q. Wang, X. S. Chen and G. Feng, *J. Phys. Chem. C*, 2015, **119**, 14167.
13   H. X. Wang, Y. R. Zhao, F. Y. Chen, Z. L. Tao and J. Chen, *Catal. Sci. Technol.*, 2016, **6**, 3443.
14   Q. Xu and M. Chandra, *J. Power Sources*, 2006, **163**, 364.
15   D. H. Sun, V. Mazumder, Ö. Metin and S. H. Sun, *ACS Nano*, 2011, **5**, 6458.
16   T. Umegaki, J.-M. Yan, X.-B. Zhang, H. Shioyama, N. Kuriyama and Q. Xu, *Int. J. Hydrogen Energy*, 2009, **34**, 3816.
17   Y. Li, Y. Dai and X. K. Tian, *Int. J. Hydrogen Energy*, 2015, **40**, 9235.
18   M. X. Li, J. T. Hu, Z. X. Chen and H. B. Lu, *RSC Advances*, 2014, **4**, 41152.
19   Y. Chen, Y. Q. Fan, Y. Pei and M. H. Qiao, *Catal. Sci. Technol.*, 2015, **5**, 3903.
20   F. Y. Qiu, L. Li, G. Liu, Y. J. Wang, C. H. An, C. C. Xu, Y. N. Xu, Y. Wang, L. F. Jiao and H. T. Yuan, *Int. J. Hydrogen Energy*, 2013, **38**, 7291.
21   J.-M. Yan, X.-B. Zhang, T. Akita, M. Haruta and Q. Xu, *J. Am. Chem. Soc.*, 2010, **132**, 5326.
22   A. J. Amali, K. Aranishi, T. Uchido and Q. Xu, *Part. Part. Syst. Charact.*, 2013, **30**, 888.
23   D. Y. Xu, P. Dai, X. M. Liu, C. Q. Cao and Q. J. Guo, *J. Power Sources*, 2008, **182**, 616.
24   H. L. Jiang, T. Umegaki, T. Akita, X.-B. Zhang, M. Haruta and Q. Xu, *Chem. Eur. J.*, 2010, **16**, 3132.
25   P. Yang, S.-Y. Jin, Q.-Z. Xu and S.-H. Yu, *Small*, 2013, **9**, 199.
26   M. Fang, Z. X. Chen, S. Z. Wang and H. B. Lu, *Nanotechnol.*, 2012, **23**, 085704.
27   H. Bai, C. Li and G. Q. Shi, *Adv. Mater.*, 2011, **23**, 1089.
28   X. H. Zhou, Z. X. Chen, D. H. Yan and H. B. Lu, *J. Mater. Chem.*, 2012, **22**, 13506.
29   M. R. Nabid, Y. Bide and F. Dastar, *Catal. Lett.*, 2015, 145, 1798.
30   J. T. Hu, Z. X. Chen, M. X. Li, X. H. Zhou and H. B. Lu, *ACS Appl. Mater. Interfaces*, 2014, **6**, 13191.
31   Z. Niu and Y. D. Li, *Chem. Mater.*, 2014, **26**, 72.
32   Y. Zhang, B. Chen, L. Zhang, J. Huang, F. Chen, Z. Yang, J. Yao and Z. Zhang, *Nanoscale*, 2011, **3**, 1446.
33   Y. J. Hu, Y. Q. Wang, Z.-H. Lu, X. S. Chen and L. H. Xiong, *Appl. Surface Sci.*, 2015, **341**, 185.
34   X. Wen, S. Q. Zhou, Q. S. Wu, J. Y. Zhang, Q. N. Wu, C. X. Wang and Y. Z. Sun, *J. Power Sources*, 2013, **232**, 86.
35   J. Li, Q.-L. Zhu and Q. Xu, *Catal. Sci. Technol.*, 2015, **5**, 525.
36   N. Cao, J. Su, W. Luo and G. Z. Cheng, *Int. J. Hydrogen Energy*, 2014, **39**, 426.
37   Ö. Metin, M. Dinç, Z. S. Eren and S. Özkar, *Int. J. Hydrogen Energy*, 2011, **36**, 11528.
38   M. Rakap, *J. Alloys Comp.*, 2015, **649**,1025.
39   F. Durap, M. Zahmakıran and S. Özkar, *Int. J. Hydrogen Energy*, 2009, **34**, 7223.
40   L. Yang, J. Su, X. Y. Meng, W. Luo and G. Z. Cheng, *J. Mater. Chem. A*, 2013, **1**, 10016.
41   Z.-H. Lu, J. P. Li, A. L. Zhu, Q. L. Yao, W. Huang, R. Y. Zhou, R. F. Zhou and X. S. Chen, *Int. J. Hydrogen Energy*, 2013, **38**, 5330.
42   R. Fernandes, N. Patel, R. Edla, N. Bazzanella, D. C. Kothari and A. Miotello, *Appl. Catal. A: General*, 2015, **495**, 23.
43   C. Z. Zhu, P. Wang, L. Wang, L. Han and S. J. Dong, *Nanoscale*, 2011, **3**, 4376.
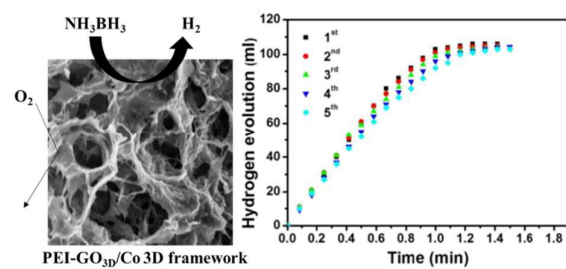
Synthesized PEI decorated GO 3D composite supported cobalt catalyst showed high catalytic activity and stability for the hydrolysis of AB.